Published in : Chemical Engineering Journal (2020), vol.397, pp. 125508
DOI: 10.1016/j.cej.2020.125508 ; Status : Postprint (Author's version)

AQUEOUS PROCESSING OF FLEXIBLE, FREE-STANDING $Li_4Ti_5O_{12}$ ELECTRODES FOR Li-ION BATTERIES

Caroline Piffet[a], Bénédicte Vertruyen[a], Sébastien Caes[a], Jean-Michel Thomassin[b], Guy Broze[b], Cédric Malherbe[c], Frédéric Boschini[a], Rudi Cloots[a], Abdelfattah Mahmoud[a]

[a]*GREENMAT, CESAM Research Unit, University of Liège, 4000 Liège, Belgium*
[b]*CERM, CESAM Research Unit, University of Liège, 4000 Liège, Belgium*
[c]*Laboratory of Inorganic Analytical Chemistry, MolSys Research Unit, University of Liège, 4000 Liège, Belgium*

Highlights

- Free-standing and flexible electrodes were prepared with an aqueous route.
- Mechanical stress on the electrode leads to better penetration of the electrolyte.
- The ratio of PEG to obtain flexible electrodes depends on its molar mass.
- PEG polymer chains probably act as spacers between PVA polymer chains.
- The best electrochemical performances were obtained for PEG 6000 (2wt%).

Abstract

The development of Li-ion batteries for the new flexible technologies should also consider environment and safety issues. Therefore, this research focused on developing an aqueous water-based process for the preparation of free-standing, CNT-free and flexible $Li_4Ti_5O_{12}$ (LTO) electrodes, where LTO itself was also obtained through an aqueous route. The electrodes contain carbon black, polyvinyl alcohol (PVA) and polyethylene glycol (PEG) 500 or 6000g/mol. The SEM and IR-ATR analyses confirmed a good distribution of all components. 2wt% PEG 6000 or 3wt% PEG 500 with respect to LTO were the optimum ratios to obtain free-standing flexible electrodes. The suspensions were studied by rheological analysis: the system was found to be stable (G' modulus above G'' modulus) and the role of the polymers and carbon in the suspensions has been investigated by viscosity measurements. Excellent electrochemical performances (up to 157mAh/g at 1C rate) were obtained for PEG6000based current-collector-free electrodes. Mild mechanical stress applied to the electrodes before the measurements allowed to enhance the performances, which could be related to the creation of tiny cracks which led to better penetration of the electrolyte in the electrode.

Keywords : Flexible electrode, Free-standing electrode Aqueous suspension, $Li_4Ti_5O_{12}$, Viscosity, Li-ion battery

1. Introduction

The minimization of energy consumption and the optimization of new strategies based on renewable energy sources rely on progress in energy storage technologies. Li-ion batteries feature prominently amongst these technologies thanks to their high energy density and long cycle-life. After conquering a near-monopoly as the power source for portable devices they are now gaining ground in the field of electric transportation.[1] Next to these widespread applications, research efforts are steadily ongoing

to develop batteries adapted to special requirements of shape, thickness, flexibility, etc. [2–5]. This often comes at the cost of some decrease in the usual battery performance indicators but is compensated by the new opportunities offered through the development of smart textiles, paper batteries, flexible batteries, etc. [6–8]. These unconventional batteries obviously benefit from processing routes that make it possible to integrate batteries wherever required. Amongst reports of paintable or printable Li-ion batteries [9–11], a striking example is the paintable $LiCoO_2/Li_4Ti_5O_{12}$ battery presented by Singh at al. [11], where all battery components (except the electrolyte) were paint-sprayed. However, this process [11] relied on NMP (N-methyl pyrrolidone)-based electrode slurries and current collectors made of carbon nanotubes (positive electrode) or copper paint (negative electrode). A safer and more environmentally friendly procedure would be to replace NMP by water and avoid carbon nanotubes [12–15]/graphene [15–18] and metallic powders [11] or foams [19]. Aqueous processing also requires the replacement of the polyvinylidene fluoride (PVDF) binder by a water-compatible alternative such as guar gum [20,21], alginate [22,23], carboxymethylcellulose (CMC) [24–27], polyacrylic acid [25,26], polyvinyl alcohol [23,25,26,28] and polyethylene glycol or derivatives [25,29]. In addition to the environmental and health benefits [30], the advantages to implement aqueous processing are also economic, since it allows a sharp decrease in solvent and binder costs (0.015$/L for water vs 1–3$/L for NMP; 2–5$/kg for CMC vs 8–10$ for PVDF according to Bresser et al. [31]).

The present work combines these different research trends into the development of a water-processed, free-standing flexible $Li_4Ti_5O_{12}$ (LTO) electrode. Carbon black (CB) is used as the electron conductor while PVA (polyvinyl alcohol) and polyethylene glycol (PEG) act as binder and plasticizer to achieve flexibility [32]. $Li_4Ti_5O_{12}$ was selected as the electrode compound in this study because it is well-known as a safe electrode material based on an abundant and environment friendly transition metal. Its insertion potential at 1.55V vs Li^+/Li is sufficiently high to avoid risks of lithium plating and the formation of a solid electrolyte interface. Three Li^+ ions insert into the structure ($Li_4Ti_5O_{12} + 3Li^+ + 3e^- \rightarrow Li_7Ti_5O_{12}$) with a quasi-null volumetric expansion. Indeed, LTO is a zero strain insertion compound. [33–37] The stability of LTO in water was studied in detail by Fongy et al. [38]: titanium dissolution was negligible at all pH while lithium dissolution did not exceed 4% after two days at natural pH in realistic mass loading conditions. The authors found that powders exposed to water and processed with NMP after drying delivered the same specific capacities at C/10, 1C and 2C rates as those of unexposed powders. The levels of lithium lixiviation observed in the present work are in agreement with the findings of Fongy et al. [38], confirming that LTO is a suitable choice for aqueous processing. Here the complete process is carried out in water since the synthesis of LTO also takes place through an aqueous spray-drying route similar to that reported in references [39–41]. Spray-drying was chosen because it enables the reproducible and easy synthesis of large quantities of electrode materials with promising electrochemical performances [42].

The first sections of the paper report on the different stages of the preparation of the flexible free-standing electrodes. Then a specific section focuses on the investigation of the role of PVA/PEG during the various stages, using rheology and other structural and morphological characterizations to build a picture consistent with the observations in the first part of the paper. Finally, the last section is dedicated to the electrode performances.

Published in : Chemical Engineering Journal (2020), vol.397, pp. 125508
DOI: 10.1016/j.cej.2020.125508 ; Status : Postprint (Author's version)

2. Material and methods

2.1. MATERIALS

TiO_2 (Degussa P25, 99.5+%), $LiOH{\cdot}H_2O$ (Alpha Aesar, 98+%), carbon black (CB, Alpha Aesar, 50% compressed), polyvinyl alcohol M_w 52000g/mol (PVA, Alcotex® with 72.5% degree of hydrolysis, Synthomer), polyethylene glycol 500g/mol (PEG 500, Clariant GmbH), polyethylene glycol 6000g/mol (PEG 6000, Merck), polyethylene glycol 10000g/mol (PEG 10000, Merck), polyethylene imine branched M_w 25000g/mol (PEI, Sigma Aldrich), N-methyl-2-pyrrolidone (NMP, Sigma Aldrich) and polyvinylidene fluoride (PVDF, Sigma Aldrich) were used as received. Deionized water was used for the preparation of all solutions and suspensions.

2.2. SYNTHESIS

The $Li_4Ti_5O_{12}$ (LTO) powder was prepared by heating at 850°C for 2h under air a precursor obtained by spray-drying an aqueous suspension of TiO_2 and $LiOH{\cdot}H_2O$ (suspension mass loading = 10wt% TiO_2, stoichiometric ratio Li:Ti = 4:5). The spray-drying parameters (Niro Mobile Minor) were as follows: inlet temperature 190°C, outlet temperature 110°C, feed rate 25mL/min, air pressure of 3 bars in the rotating injector.

In a typical experiment, the LTO powder was suspended in water (33wt% LTO in water) and ball-milled for 1h (planetary miller Retsch PM400/2, zirconia balls with a diameter of 0.5mm). Carbon black (as a 2.5wt% aqueous suspension with PEI dispersant), polyvinyl alcohol (as a 25wt% aqueous solution) and polyethylene glycol were then added to the LTO suspension to reach the following mass ratios: LTO/C/PEI/ PVA/PEG = 100/20/0.3/20/x, with x = 0 to 5. The total solid mass loading was about 12% in water. The suspension was tape-casted at room temperature on non-conductive glass plates using a motorized doctor blade (BYK byko-drive XL) at a speed of 4cm/s. The deposited area was about 10×20cm^2. After drying at room temperature, razor blades were used to remove self-supporting strips from which electrodes were cut.

In the next sections, all samples will be identified by their percentage of PEG with respect to LTO, as in the first line of Table 1. For easier reference, the mass percentages of LTO, CB, PVA and PEG in the suspensions and in the dry tapes are also collected in Table 1. The very small amount of branched polyethyleneimine (0.02wt% in suspension) originating from the carbon black suspension is not included in the table; PEI is not expected to have any negative effect on final properties since much larger amounts were successfully used in $LiFePO_4$ electrodes.[43]

Table 1. Mass percentages of LTO, CB, PVA and PEG in suspension and in the dry tapes.

	LTO	CB	PVA	PEG	Water
wt% with respect to LTO	100	20	20	0 – 1 – 2 – 3 – 4 – 5	–
wt% in suspension	8.5	1.7	1.7	0 – 0.08 – 0.17 – 0.25 – 0.33 – 0.4	88
wt% in dry tape	70	14	14	0 – 0.7 – 1.4 – 2.1 – 2.8 – 3.5	–

Published in : Chemical Engineering Journal (2020), vol.397, pp. 125508
DOI: 10.1016/j.cej.2020.125508 ; Status : Postprint (Author's version)

2.3. CHARACTERIZATIONS

Powder X-ray diffraction was performed in Bragg-Brentano geometry using a Bruker D8 Twin-Twin diffractometer with Cu K_{alpha} radiation. In order to determine the amorphous content, accurately weighted amounts of the LTO powder and an Al_2O_3 internal standard were carefully mixed and the diffractogram of the mixture was fitted with the TOPAS software using the fundamental parameters approach to model the instrumental contribution [44]. The scale factors, background and profile parameters were refined while the cell parameters, atomic positions and occupation factors were taken from references 04–009-5069 ($Li_4Ti_5O_{12}$) and 00–046-1212 (Al_2O_3) of the PDF-4+ database (International Center for Diffraction Data). The amorphous content was computed by imposing that the weight percentage of internal standard be equal to that of the powder mixture [45]. Inductively coupled plasma – optical emission spectrometry (ICP-OES) analyses were performed with a Varian spectrometer. The morphological properties and particle sizes were measured by laser diffraction granulometry (Malvern Mastersizer 2000 Hydro) and scanning electron microscopy (ESEM Philips XL-30 at 15kV). The specific surface area was determined with a Micromeritics Asap 2020 Plus instrument. Degassing was applied for 180min at 150°C with a heating ramp of 10°C/min. The adsorption measurement was performed by the Rouquerol method under N_2 from 0 to 0.3 with a 0.03 step. Infrared spectra were collected with a Thermo Fisher Scientific Nicolet spectrometer iS5 ATR iD7 system with a germanium crystal. DSC measurements were performed on a Q100 from TA instruments, the first cycle from −80°C to 120°C and the second cycle from −80°C to 200°C. The optical micrographs were obtained with a Nikon SMZ1500 Stereoscopic Zoom Microscope. The viscosity and stability of the suspensions were measured with an Anton Paar rheometer MCR 102 using a double gap cylinder. Rotational tests were performed from 0.1 to 100s^{-1} and directly afterwards from 100 to 0.1s^{-1}. The linear viscoelastic (LVE) domains were determined by an amplitude oscillation test (0.01–200%) at a 10rad/s frequency. Then the frequency oscillation tests (100–0.1rad/s, logarithmic ramp) were performed at the LVE limit. The zeta potential was measured with zetameter DT-1200. The electrochemical measurements were performed in Swagelok type cells with a BioLogic VMP3 potentiostat/galvanostat in a voltage window of 2.5–1V vs. Li^+/Li. Cells were assembled in a glove box after drying the working electrodes at 110°C for 12h under vacuum. Metallic lithium was used as counter and reference electrode. The electrolyte was $LiPF_6$ 1M in ethylene carbonate:dimethyl carbonate (1:1 in volume), the separator consisted of a polypropylene membrane (Celgard). All electrochemical tests were carried out at room temperature.

3. Results and discussion

3.1. BALL-MILLING OF $LI_4TI_5O_{12}$ IN WATER

The LTO particles obtained by heat treatment of the spray-dried powders were too large to be stable in suspension. The LTO particles size was therefore reduced from 10.5µm to 0.6µm (d0.5 values) by ball-milling in water for one hour, as shown in the particle size distribution in Fig. 1a and confirmed by the scanning electron micrograph in Fig. 1b (see Fig. S1 shows SEM images of the LTO powder before ballmilling). The XRD pattern of the ball-milled powder (Fig. 1c) does not reveal any secondary phase and Rietveld refinement in presence of an internal standard did not evidence any significant amorphization (Fig. S2). The small increase in the width of the XRD reflections can be interpreted as a decrease in crystallite size from 113 ± 22nm before ball-milling to 51 ± 5nm after ball-milling (see Fig.

S2 for XRD pattern of the LTO powder before ball-milling). ICP analysis was used to quantify that about 2.5mol% of the lithium in the LTO phase was lost by lixiviation during ball-milling. After the whole suspension preparation, this amount reached 3.7mol%. These values are consistent with the results of Fongy et al [38] in their study of LTO aqueous suspensions. The natural pH of the suspension after milling was 12 and zeta potential was −53mV. The basic pH means that the extensive Li^+/H^+ exchange that has been reported in acidic medium by Simon et al [46] would not be a major contribution in the present case. The negative value of the zeta-potential and basic pH can be rationalized based on the following equation, which takes into account Li^+ lixiviation and the acid/base character of surface oxygens:

$$Li_4Ti_5O_{12(surface)} + y\ H_2O \rightarrow [Li_{4-x}Ti_5O_{12-y}(OH)_y]^{(x-y)-} + x\ Li + y\ OH^-$$

However, the observation that the Li^+ concentration is about 10 times higher than the OH^- concentration in the milling water suggests that a significant fraction of the lithium ions in solution could result from the dissolution of an undetected amorphous Li-rich surface layer (see the work by Gao et al. [47] on surface carbonatation/hydroxylation of stored LTO). Since Li^+ lixiviation occurs primarily in the surface layer, information on the average composition (Li/Ti = 0.77 vs. 0.8 for stoichiometric $Li_4Ti_5O_{12}$) is usefully complemented by considering a simplified model where lithium lixiviation results in a TiO_2 surface layer, the thickness of this layer in the present case would be 4nm for LTO particles with a diameter of 600nm. It has been reported that a small amount of TiO_2 can be beneficial for the electrochemical performances of LTO [48,49]. In order to assess the consequences on electrochemical performance in the present case, some ball-milled LTO suspension was lyophilized and an electrode on Cu foil was prepared using a standard procedure, i.e. mixing LTO with carbon black and PVDF in NMP, with the following ratio: LTO/CB/PVDF = 70/15/15. The specific capacities and rate capability reported in Fig. 1d are comparable to results obtained when ball-milling is carried out in a non-aqueous medium, demonstrating the suitability of the aqueous procedure for the preparation of LTO electrodes. [33,34]

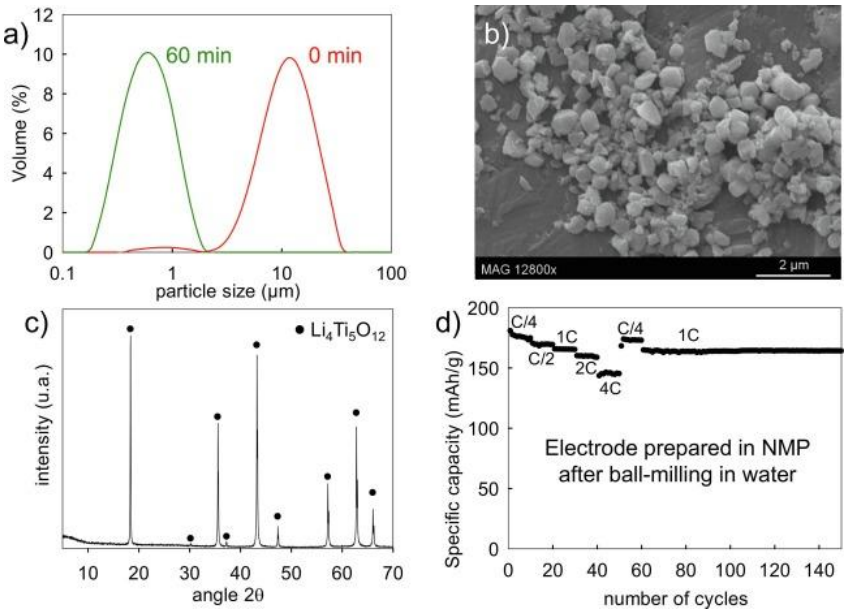

Fig. 1. *Characterization of the LTO powder after 60min ball-milling in water: (a) Particle size distribution before and after ball-milling, as measured by laser granulometry. (b) Secondary electron micrograph after ball-milling. (c) XRD pattern. (d) Electrochemical performance of LTO ball-milled in water, dried and dispersed in NMP for electrode preparation (voltage range: 2.5–1V vs Li^+/Li; LTO mass loading: 2.20mg/cm^2; electrode thickness: 17µm on Cu current collector).*

Published in : Chemical Engineering Journal (2020), vol.397, pp. 125508
DOI: 10.1016/j.cej.2020.125508 ; Status : Postprint (Author's version)

3.2. SUSPENSION FORMULATION

After mixing the LTO suspension with the aqueous carbon black suspension (LTO/CB with a ratio 100/20 in weight, see Materials and methods for details), water-compatible additives were required so that current-collector-free tapes could be doctor-bladed.

After extensive preliminary testing, polyvinyl alcohol (PVA – see specifications in Materials and Methods) in 20wt% ratio with respect to LTO was selected as binder. Polyethylene glycols (PEG) with various chain lengths were tested as plasticizers by adding them in different mass ratios to the suspension. Please note that, as previously mentioned in Section 2.2, all suspensions and samples are identified by their percentage of PEG with respect to LTO (first line of Table 1). The selection criterion was based on the presence or absence of cracks in the dry tapes, as shown in Fig. 2. PEG 10000 was immediately dismissed because inhomogeneities and cracks in the tapes, combined with very high suspension viscosity, revealed that the chain length was too large for PEG 10000 to act as a plasticizer. In the case of suspensions containing PEG 500, the dry tapes containing from 0 to 2wt% PEG 500 were severely cracked. From 3 to 5wt% PEG 500, the tapes displayed no cracks and were flexible (see later). As the LTO ratio should be the highest in the electrode, 5wt% PEG 500 tapes will not be considered. Indeed, 3wt% of PEG 500 is enough to ensure the electrode flexibility. The results for suspensions containing PEG 6000 followed similar trends but the optimal range of PEG content was narrower. The tapes obtained with 2% of PEG 6000 were crack-free and flexible but higher contents in PEG 6000 led to cracks and inhomogeneities in the dry tapes. These results, together with rheological data, will be included in the general discussion of the role of PVA and PEG in a later section of the paper.

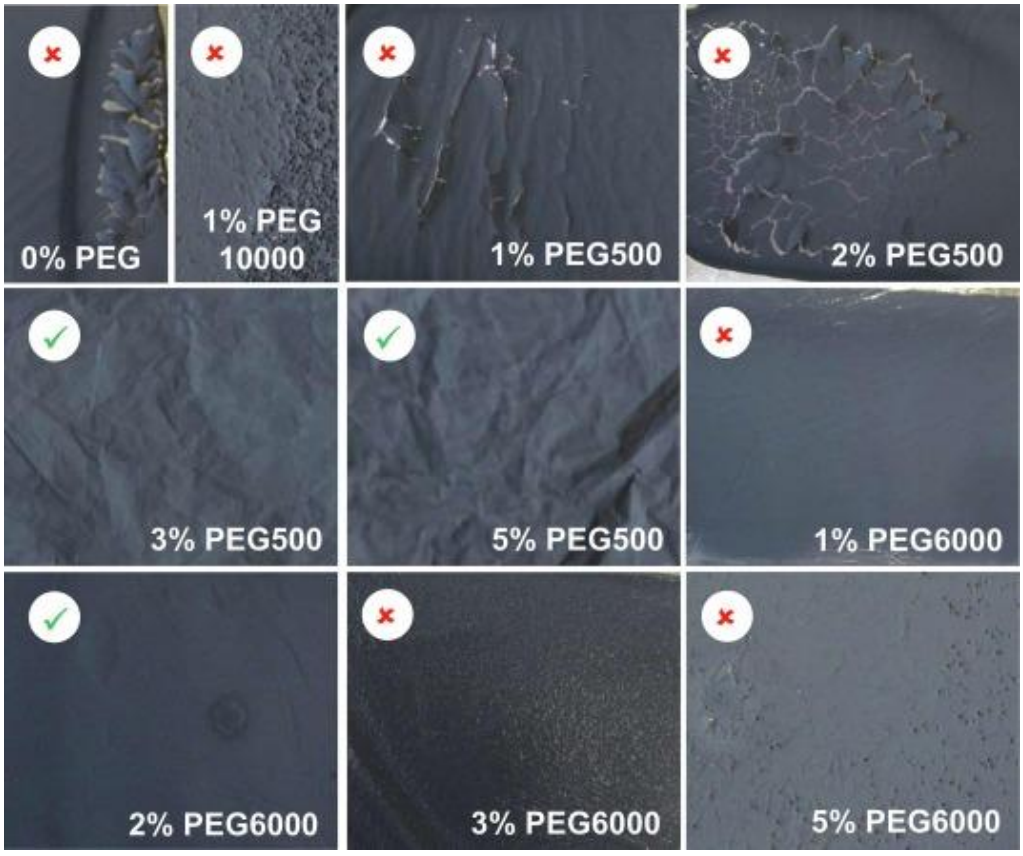

***Fig. 2**. Photographs of LTO-C-PVA-PEG tapes (about 5x6cm^2) with 20wt% PVA with respect to LTO and different contents of PEG.*

Published in : Chemical Engineering Journal (2020), vol.397, pp. 125508
DOI: 10.1016/j.cej.2020.125508 ; Status : Postprint (Author's version)

3.3. TAPE MICROSTRUCTURE AND FLEXIBILITY

Tapes casted from suspensions containing 3wt% PEG 500 (photograph presented in Fig. S3) or 2wt% PEG 6000 (with respect to LTO) could be peeled off the glass substrate and were found to be flexible and macroscopically crack-free. Tapes were prepared from several batches over the course of the research project and the results were consistent and reproducible between batches. Fig. 3 shows optical micrographs of the tapes to examine them at higher magnification in the as-obtained state and after submitting them to mechanical stress, i.e., rolling around a 4mm diameter cylinder or folding. Before applying mechanical stress, the micrographs of the tapes are very similar. The darker zones correspond to local depressions in the tape surface and no microstructural difference between these zones and the rest of the tape were observed by electron microscopy. After rolling the tapes around a 4mm diameter cylinder, the optical micrographs did not reveal any significant changes. After folding, a few cracks appeared in the PEG6000-based tape while the PEG500-based tape seemed unchanged.

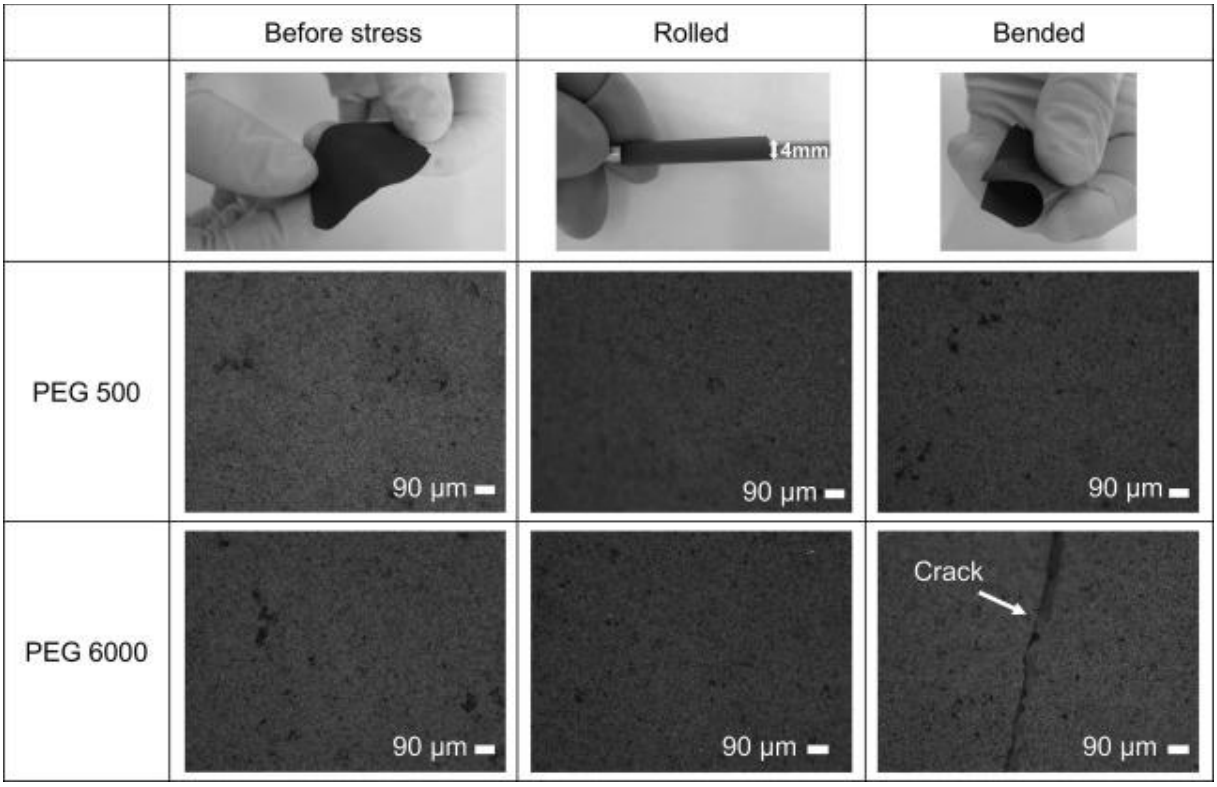

Fig. 3. *Optical micrographs of the surfaces of LTO-C-PVA-PEG tapes with 3wt% PEG 500 or 2wt% PEG 6000, in the as-obtained state, after a rolling test and after a folding test.*

The electrodes cut from the tapes were characterized at higher magnification by scanning electron microscopy (Fig. 4). EDX analysis coupled to the electron microscope was also used to assess the electrode homogeneity. Fig. 4 presents results for the electrode containing 3wt% PEG 500, similar micrographs were obtained for electrodes with 2wt% PEG 6000. The dispersion of the LTO and carbon black particles is comparable to electrodes prepared by the standard procedure using dispersion in NMP and deposition on a current collector. Fig. 4g shows that for electrodes with thickness ranging between 20 and 70µm, the electrode mass (in mg/cm^2) is proportional to its thickness (linear regression with $r^2 = 0.93$), indicating that the packing density observed in the micrographs of Fig. 4 is similar for all tapes. The tape surface that was in contact with the glass substrate during doctor blading is visibly smoother (see Fig. S4) than the other side but the time of penetration of a droplet of

Published in : Chemical Engineering Journal (2020), vol.397, pp. 125508
DOI: 10.1016/j.cej.2020.125508 ; Status : Postprint (Author's version)

electrolyte is similar for the two sides. The binder distribution in the LTO-C-PVA-PEG6000 and LTO-C-PVA-PEG500 flexible tapes is good enough that no loose powder is released when handling the tapes. Moreover, the IR spectra collected at several random positions of the two faces of the electrode reveal a homogenous distribution of the polymers in the electrode (see Fig. S5 and peak assignment [50–54] in Table S1).

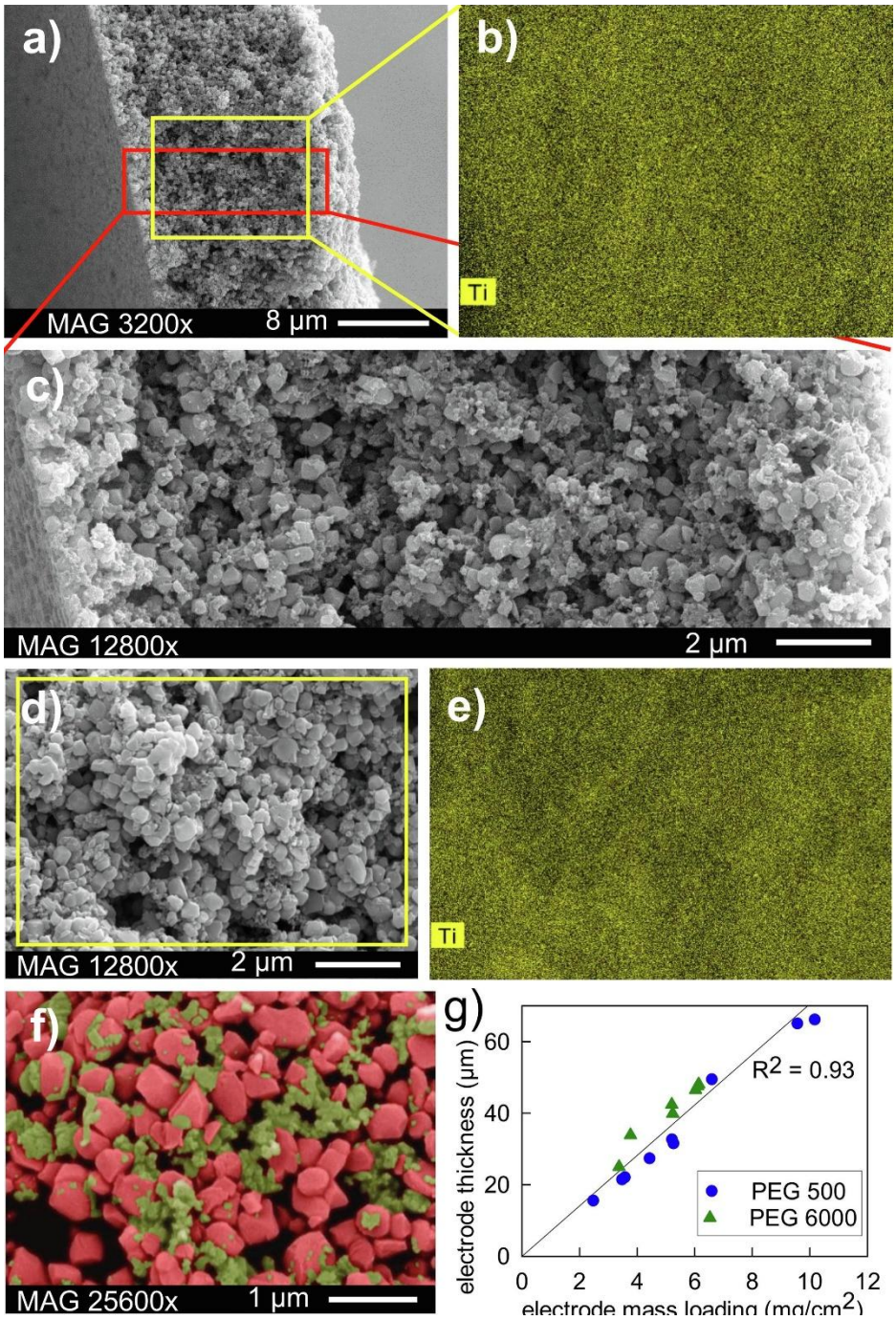

Fig. 4. *SEM micrographs of a LTO-C-PVA-PEG electrode with 3wt% PEG 500. (a,b,c) Cross section micrographs and EDX map of the titanium signal. (d,e,f) Surface micrographs and EDX map of the titanium signal; in (f), $Li_4Ti_5O_{12}$ particles were colored in red and carbon black particles in green. (g) Electrode thickness (µm) as a function of mass loading of the electrode (mg/cm^2).*

Published in : Chemical Engineering Journal (2020), vol.397, pp. 125508
DOI: 10.1016/j.cej.2020.125508 ; Status : Postprint (Author's version)

3.4. INVESTIGATING THE ROLE OF PVA/PEG

This section reviews the previous results in the light of rheological measurements and differential scanning calorimetry (DSC) data collected to investigate the role and behavior of PVA and PEG in the suspensions and in the tapes.

Fig. 5 shows the rheological data for suspensions containing 3wt% PEG 500 or 2wt% PEG 6000 with respect to LTO, i.e., two of the suspensions that result in flexible crack-free tapes. Tests in rotation conditions were performed by measuring viscosity as a function of shear rate. As shown in Fig. 5a, the viscosity decreased with increasing shear rate (shear-thinning behavior). The deformation reached at high shear rate was reversible since the two curves superimpose at low shear rates. The stability of the suspension at rest (i.e., during storage or during tape drying) was characterized by measuring the storage modulus (G') and the loss modulus (G'') in oscillatory mode while sweeping the frequency from 0.1 to 100 rad/s. In order to select an oscillation amplitude corresponding to a strain within the linear viscoelastic region (LVE), the LVE limit had been previously determined (not shown) by amplitude sweep measurements at 10 s^{-1} oscillation frequency. Discussion of the LVE limit is postponed to the next paragraph. Fig. 5b shows that the storage modulus G' was higher than the loss modulus G'' in the whole frequency range, reflecting a solid-like behavior of the suspension in the tested frequency domain over the time-scale of the test. The elastic component being higher than the viscous component is consistent with the high viscosity measured at low shear rate. The absence of any irreversible evolution in the mixing of the different components was confirmed by measuring viscosity every day during one week after stirring the settled suspension for 15 min and observing only negligible variations in the viscosity versus shear rate curves (see figure S6). These results are further corroborated by the homogeneous distribution of LTO and CB across the tape thickness revealed in the micrographs of cross-sections such as shown in Fig. 4.

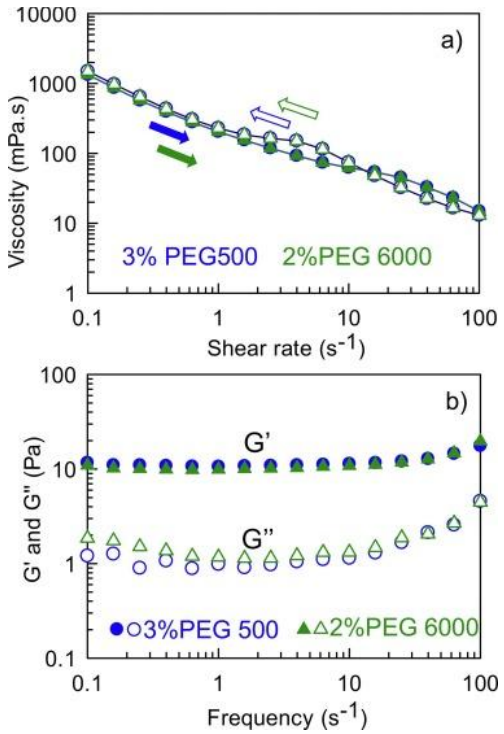

Fig.5. *Rheological data for LTO-C-20wt%PVA-PEG suspensions with 3wt% PEG 500 or 2wt% PEG 6000: (a) Viscosity versus shear rate from 0.1 to 100s^{-1} and from 100 to 0.1s^{-1} ; (b) Evolution of the storage (G') and loss modulus (G'') in a frequency sweep test from 0.1 to 100rad/s (0.1% deformation).*

Published in : Chemical Engineering Journal (2020), vol.397, pp. 125508
DOI: 10.1016/j.cej.2020.125508 ; Status : Postprint (Author's version)

The small values of the LVE limit (0.2% and 0.4% for the suspensions containing 3wt% PEG 500 or 2wt% PEG 6000 with respect to LTO, respectively) suggest that the C and/or LTO particles participate in the network that imparts a solid-like behavior to the suspensions for short time-scales. This was further studied through viscosity measurements on LTO/C/PVA suspensions where either LTO or C was removed from the formulation, while keeping the same amounts of PVA and water. The mass loading of these LTO-PVA and C-PVA suspensions were 10wt% and 2wt%. Fig. 6a shows that the suspension viscosity decreased more strongly if the carbon black was removed from the formulation than if LTO was removed, although the carbon black represents a smaller mass percentage than LTO. This can be explained by the small particle size and high surface area of the carbon black. Indeed, the carbon black used in the present work was studied in detail by Parant et al. [55], who observed dense primary particles of about 100nm diameter aggregated into filamentous, fractal-like structures. Another characteristics of this carbon black [55] is its almost zero zetapotential in water at all pH, due to the hydrophobic character imparted by a low functionalization level (only 0.4% oxygen detected by XPS). In the suspensions studied here, the involvement of the carbon black particles in the solid-like network is probably mediated by the PEI that was used to disperse it in the first place, and/or by adsorption of PEG or PVA through interactions with the lower-polarity segments of the polymer chains.

Fig. 6 b illustrates some results from the preliminary tests for several contents of PVA, where it can be seen that the suspensions with 20wt% PVA displayed a lower viscosity than the suspensions with only 10wt% PVA. This might be related to a decrease in bridging effects when more PVA chains are available to interact with the carbon or LTO particles, providing better steric stabilization and easier motion within the system when shear stress is applied.

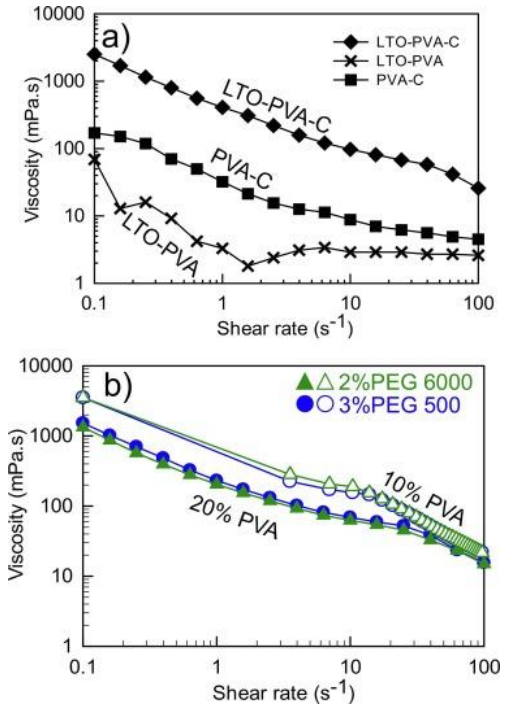

Fig. 6. *(a) Comparison of the viscosity versus shear rate curves for suspensions containing respectively LTO-C-PVA, C-PVA or LTO-PVA (see text for details); (b) Comparison of viscosity versus shear rate curves for LTO-C-PVA-PEG suspensions containing either 10wt% or 20wt% PVA.*

Published in : Chemical Engineering Journal (2020), vol.397, pp. 125508
DOI: 10.1016/j.cej.2020.125508 ; Status : Postprint (Author's version)

The effect of the PEG content over the viscosity vs. shear rate curves (Fig. 7) was studied for a PVA content of 20wt%. For each ratio of PEG 500 or 6000 tested, the resulting suspension has a shear-thinning behavior. In the case of PEG 500, the variation in viscosity was negligible for PEG contents up to 2wt% followed by a drop to lower values for PEG contents of 3–5wt%. In the case of PEG 6000, the curves shifted progressively to lower viscosity values for PEG content increasing from 0 to 2wt% while for PEG content of 3wt% and above the suspensions became more viscous than the PEG-free formulation. Fig. 7c plots the viscosity values at a shear rate of $65s^{-1}$, corresponding to the velocity/ gap ratio of the tape casting process. There is a systematic correlation with the presence/absence of cracks in the dry tapes (see photographs in Fig. 2), with an apparent threshold value around 20mPa.s. Another quantitative value that can be extracted from the rheology measurements is the yield stress (determined from a linear fit in the shear stress vs. shear rate plots, see Fig. S7 and Table S2); when plotted against PEG content, it can be seen that crack-free flexible tapes are obtained when the yield stress does not exceed about 500mPa.

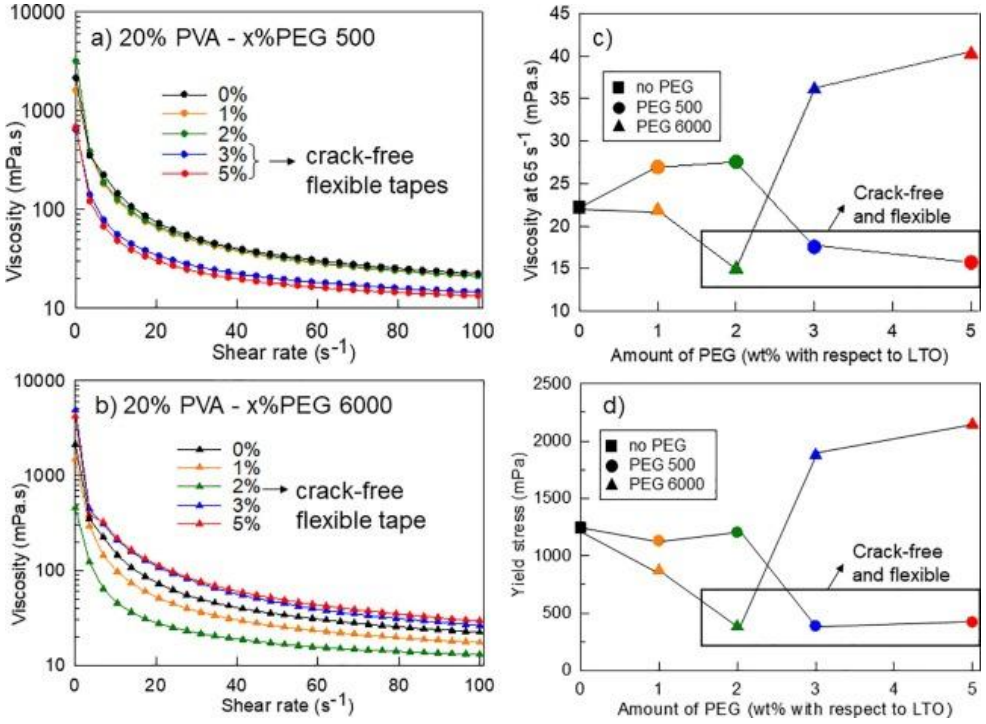

Fig. 7. *LTO-C-PVA-PEG suspensions: (a) Viscosity versus shear rate curves for suspensions with PEG 500; (b) Viscosity versus shear rate curves for suspensions with PEG 6000; (c) Viscosity at $65s^{-1}$ versus PEG content; (d) Yield stress versus PEG content.*

In order to gain indirect insights into the interactions of PEG with PVA in the suspensions, DSC analyses (Fig. 8) were performed under air on a LTO-C-PVA-PEG6000 tape and compared to data collected for tapes casted from aqueous solutions of PVA and/or PEG. The DSC curve for the PVA-only film (52.000g/mol, polydispersity 2.39 according to supplier) showed a glass transition temperature (T_g) at about 60°C and two endothermic peaks at 130°C and 170°C, tentatively assigned to the crystallization of PVA segments with different degrees of hydrolysis. Addition of PEG500 or PEG6000 to PVA in the same mass ratios as in the LTO-C-PVA-PEG tapes led to a suppression of the PVA crystallization peaks. This suggests that the PEG chains intermingled with the PVA chains by interfering in the hydrogen bonding network of the alcohol moieties of PVA. This interpretation is supported by the work of Li et al. [56] about the interactions between PVA and PEG segments in PVA-PEG membranes. In the case of

PVA 1700 g/mol and different PEG with molar mass 200, 400 and 600g/mol, these authors proposed that PEG species increase the spacing between the PVA chains and form PEG-PVA hydrogen bonds. Another relevant parallel with literature is the fact that using PEG as plasticizer for PVA in Li-polymer electrolytes has been shown to increase the polymer chain mobility and the ionic conductivity [57,58]. However, the PVA-PEG6000 film also displayed a sharp peak at about 58°C, which can be attributed to the crystallization of part of the PEG6000. This assignment is corroborated by the absence of such a peak in the PVA-PEG500 film, since PEG500 is known to be amorphous at room temperature. This crystallization peak of PEG6000 is also observed in the DSC curve of the LTO-C-PVA-PEG6000 electrode, suggesting that above some ratio of PEG 6000 to PVA, the formation of PEG 6000 agglomerates becomes more favorable than its participation to a PEG-PVA network. These DSC results for the dry tapes can be used as guidelines to discuss the rheology of the suspensions in Fig. 7. In the case of PEG 500, the small size of the PEG chains by comparison with the PVA chains could explain why a threshold value has to be exceeded to observe an effect on the suspension viscosity; in the case of PEG 6000 the marked increase in viscosity above the optimum PEG content could be explained by agglomeration of PEG 6000, leading to a lower effective content of PEG in interaction with PVA. The less efficient plasticization due to the existence of PEG6000 crystallites in the dry tapes would also provide an explanation for the observation in Fig. 3 that a few macrocracks appeared in the PEG6000 based electrode after folding while it was not the case for the PEG500-based electrode.

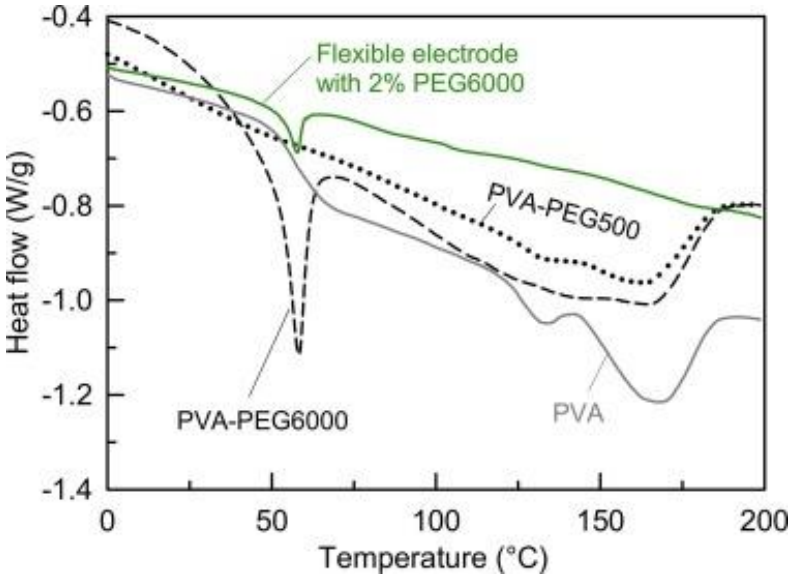

Fig. 8. *DSC analysis in the temperature range of −80–200 °C for the LTO-C-PVA-PEG6000 flexible electrode and for PVA, PVA-PEG6000 and PVA-PEG500 blends in the same ratios as in the corresponding flexible electrodes.*

3.5. ELECTROCHEMICAL PROPERTIES

The free-standing flexible electrodes with 2wt% of PEG 6000 and 3wt% of PEG 500 were tested in half-cell configuration against a Li counter-electrode (Fig. 9). Electrodes were cut both from as-obtained tapes and from tapes submitted to a rolling procedure (see Fig. 3). As shown in Fig. 9a where the electrochemical tests for more than 10 electrodes are collected, the discharge capacity at C/4 was almost consistently above 150mAh/g (comparable to literature for spray-dried LTO [40,59,60] and for processing in water [22,61]) and reached theoretical capacity for the best samples. The same figure

does not reveal any trend associated to mass loading in the investigated range. This result confirms that electrodes with high mass loadings also exhibited good electrochemical performance.

The rate capability test (see representative results in Fig. 9b) allowed to differentiate between the electrodes, with the rolled PEG6000 electrodes systematically performing better than the other electrodes (up to 162mAh/g, 157mAh/g, 136mAh/g and 109mAh/g at C/4, 1C, 2C and 4C rates respectively). The discharge capacity was retained during the 10 performed cycles at all C-rates for all samples. The improvement of performance in rolled electrodes was also observed for PEG500 electrodes and will be discussed in the next paragraph. For meaningful comparison, the performances of the rolled PEG6000 electrodes should be compared to other current-collector-free and/or flexible and/or water-processed LTO electrodes reported in the literature (Table 2). It should be noted that, in contrast to our work, all freestanding and/or flexibles electrodes in Table 2 contain either CNT, graphene or reduced graphene oxide (rGO). These carbon sources are reported to be more expensive and/or toxic than carbon black [62]. The flexible and free-standing electrodes produced by Bourgeois et al. [13] reach 145mAh/g at 1C rate, with 15wt% carbon nanotubes acting both as binder and electron conductor. The free-standing electrodes reported by Cao et al. [63] display 145mAh/g at 1C rate with 70wt% of LTO and CNT as electron conductor. Up to 2C-rate, the rolled PEG6000 CNT-free electrodes developed by an aqueous and non-toxic procedure in this work performed slightly better (157mAh/g) than these two electrodes and were topped only by electrodes based on LTO-graphene [19] or LTO-rGO [16] composites synthesized by much more complex procedures (see Fig. S8 for a comparison of rate capabilities). Table 2 also shows that the rolled PEG6000 CNT-free electrodes compete favorably with some water-processed electrodes on metallic current collectors.

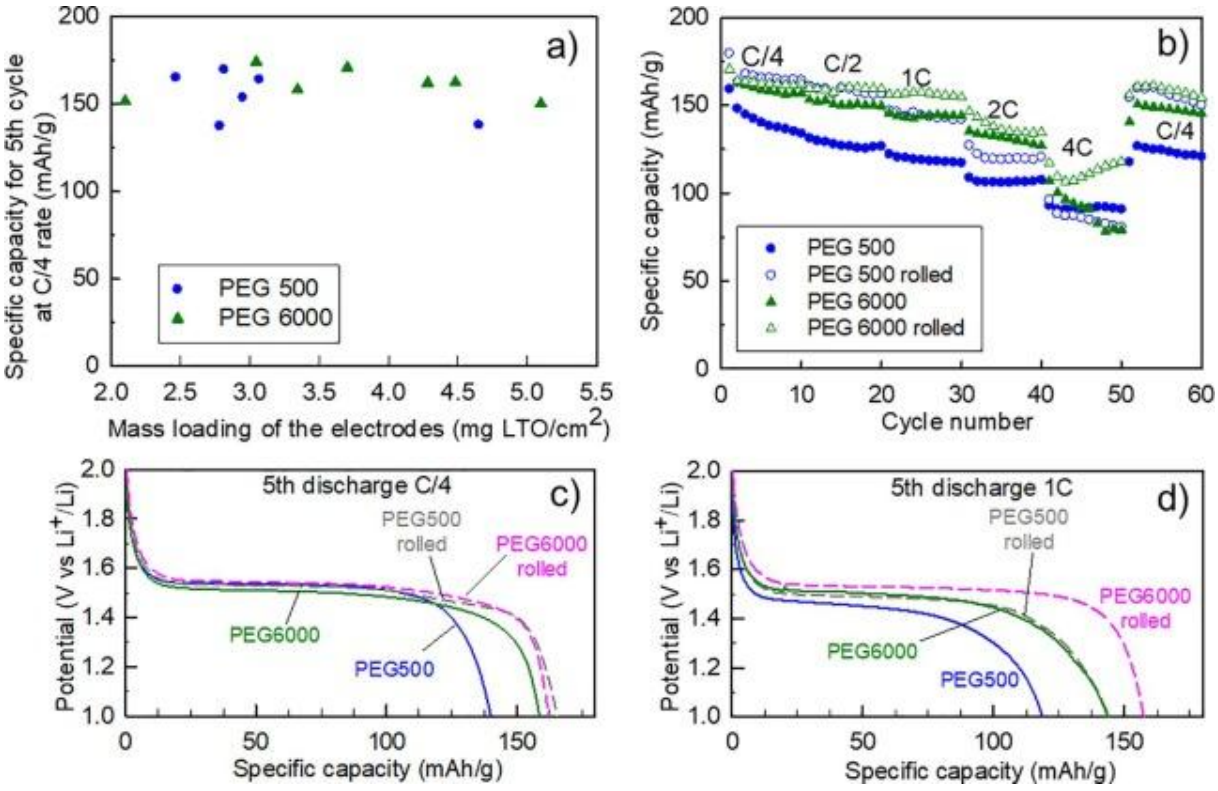

Fig. 9. *Electrochemical tests on LTO-C-PVA-PEG free-standing electrodes with 3wt% PEG 500 or 2wt% of PEG 6000. (a) Specific capacity at C/4 plotted vs mass loading of the electrode. (b) Electrochemical cycling at different current densities. (c) Electrode capacity for the 5th cycle at C/4 cycling rate. (d) Electrode capacity for the 5th cycle at 1C cycling rate.*

Looking in more detail at the discharge curves in Fig. 9c and d shows that the electrodes that display a significant decrease in capacity from C/4 to 1C are also characterized by a higher polarization (decrease of the working voltage) and shorter insertion plateau. This suggests that the excellent performance of the rolled PEG6000 electrodes is due to characteristics influencing the kinetics of charge transport. The most likely reason is that rolling creates microcracks in the polymer matrix, thereby allowing a better penetration of the electrolyte into the electrode and faster lithium diffusion. This is supported by the observation that the performance of rolled PEG500 electrodes is less degraded at cycling rates up to 2C than that of not-rolled PEG500 electrodes. The reason for achieving better performance of rolled PEG6000 electrodes compared to rolled PEG500 electrodes is difficult to precise unambiguously because, in mass percentage, PEG is a minor component in the electrode (2wt% for PEG6000 vs. 3wt% for PEG500). The fact that the folding test, which is more severe than the rolling test, creates some cracks in the PEG6000 electrode (see optical micrographs in Fig. 3) has been tentatively linked to the presence of PEG6000 crystallites evidenced by thermal analysis (section 3.4) and suggest that microcracking during rolling could be more extensive in the PEG6000 electrodes and induce better electrolyte penetration which will shorten the lithium during charge/discharge process.

4. Conclusions

This work successfully combined a preparation process in water and free-standing flexible LTO electrodes. We prepared LTO aqueous suspensions with carbon black, PVA and PEG additives. The impact of PEG molar mass and of the polymer ratio on the flexibility of the freestanding electrodes was evidenced. It was shown that 3wt% PEG 500 or 2wt% PEG 6000 (with respect to LTO) yield to crack free and free-standing electrodes. The SEM and IR-ATR analyses of these two electrodes demonstrated a homogenous distribution of all electrode components.

The role of the polymers in the slurries was investigated by rheological measurements. A correlation was evidenced by the presence or absence of cracks in the dry tapes. All suspensions displayed a shear-thinning behavior. Oscillation tests showed a stable system with G' modulus above G'' modulus. Viscosity measurements gave information about the role of PVA, C and PEG in the suspensions, suggesting that the stability of the system is related to the high surface area of the carbon black and the sufficient amount of PVA. PEG appeared to act as a spacer between the PVA chains, suppressing the formation of cracks when the correct amount is used (2wt% for PEG6000 or 3wt% for PEG500). If a too large quantity of PEG6000 was used, the plasticization effect was lost because of crystallization.

Excellent electrochemical performances of our free-standing flexible electrodes at reasonably low cycling rates were reached for electrodes that display high intrinsic flexibility without any need of any substrate and do not include CNT (toxic and expensive additive). The capacities with PEG6000 as plasticizer were higher than with PEG500 despite the latter being a better plasticizer, probably because of the presence of small cracks promoting electrolyte penetration. The mechanical stress on the electrode had a beneficial effect on the electrochemical performances of the electrodes probably thanks to the formation of additional small new cracks.

In summary, the aqueous eco-friendly and cheap formulations developed in this study represent promising results for implementation in flexible batteries. It is expected that the PVA-PEG matrix developed for LTO could be implemented for graphite and other anode materials whose lower potentials would result in slightly less safe but more efficient batteries with higher energy density. The stability of the anode material during the aqueous processing would be the limiting factor (for example, Li_3VO_4 is reported as strongly hydrophilic [64]), since both PVA and PEG polymers have already demonstrated electrochemical stability as a binder for graphite electrode (PVA)[65] or in polymeric solid electrolytes (PEG) [66].

Published in : Chemical Engineering Journal (2020), vol.397, pp. 125508
DOI: 10.1016/j.cej.2020.125508 ; Status : Postprint (Author's version)

Table 2. Comparison of published values of specific capacity at 1C rate for water-processed and/or current-collector-free and/or flexible $Li_4Ti_5O_{12}$ electrodes.

Abbreviations: LTO = $Li_4Ti_5O_{12}$; CNT = carbon nanotubes; CNF = cellulose nanofiber; CB = carbon black; rGO = reduced graphene oxide; NMP = N-Methyl-2-pyrrolidone; PVDF = polyvinylidene fluoride; PEG = polyethylene glycol; CMC = carboxymethyl cellulose; NBR = butadiene-acrylonitrile copolymer rubber latex.

Material	Solvent	Binder	Conductive carbon additive	Current collector	Reported as flexible	Specific capacity at 1C rate	First author	Ref
LTO	Water	PVA/PEG	CB	None (free-standing)	Yes	157 mAh/g	Piffet	This work
LTO	Butanol	/	CNT	None (free-standing)	Yes	130–145 mAh/g, depending on the sample	Bourgeois	[13]
LTO-graphene	/	/	graphene foam from the material	None (free-standing)	Yes	175 mAh/g	Qian	[19]
LTO-rGO	/	/	/	None (free-standing)	Yes	177 mAh/g	Zhu	[16]
LTO/CNT/CNF	Water	CNF	CNT	CNT/CNF coating on the LTO/CNT/CNF layer	Yes	146–156 mAh/gdepending on the sample	Cao	[63]
LTO	Water	guar gum	CB	Al	No	170 mAh/g	Carvalho	[21]
LTO	Water	pectin	CB	Al	No	171 mAh/g	Carvalho	[21]
LTO	Water	CMC	CB	Al	No	166 mAh/g	Carvalho	[21]
LTO	Water	Sodium alginate	CB	carbon-coated Al	No	141–165 mAh/g, depending on the sample	De Giorgio	[22]
LTO	Water	Sodium alginate	CB	Cu	No	112 mAh/g	Phanikumar	[23]
LTO	Water	PVA	CB	Cu	No	140 mAh/g	Phanikumar	[23]
LTO	Water	PEG-based polymer	CB	Ni foam	No	130–142 mAh/g, depending on the sample	Tran	[29]
LTO	Water	CMC/NBR/Triton X-100	CB	Al	No	110–143 mAh/g, depending on the sample	Fongy	[38]

Declaration of Competing Interest

The authors declare that they have no known competing financial interests or personal relationships that could have appeared to influence the work reported in this paper.

Acknowledgments

The authors are grateful to University of Liege and FRS-FNRS for equipment grants. Part of this work was supported by the Walloon Region under the "PE PlanMarshall2.vert" program (BATWAL – 1318146). The authors thank Synthomer for providing for free Alcotex® polymers. The authors also thank Tania Costanza and Thomas Jungers for collaboration, Amélie Corato and Audrey Schrijnemakers for their help for the utilization of optical microscope and BET respectively. Electron microscopy was carried out at the CAREM platform (University of Liège).

Appendix A. Supplementary data

Supplementary data to this article can be found online at https:// doi.org/10.1016/j.cej.2020.125508.

5. References

[1] T. Kim, W. Song, D.Y. Son, L.K. Ono, Y. Qi, Lithium-ion batteries: outlook on present, future, and hybridized technologies, J. Mater. Chem. A. 7 (2019) 2942–2964, https://doi.org/10.1039/C8TA10513H.

[2] A. Vlad, N. Singh, C. Galande, P.M. Ajayan, Design Considerations for Unconventional Electrochemical Energy Storage Architectures, Adv. Energy Mater. 5 (2015) 1–53, https://doi.org/10.1002/aenm.201402115.

[3] Y. Li, R. Wang, Z. Guo, Z. Xiao, H. Wang, X. Luo, H. Zhang, Emerging TwoDimensional Noncarbon Nanomaterials for Flexible Lithium-Ion Batteries: Opportunities and Challenges, J. Mater. Chem. A. 7 (2019) 25227–25246, https:// doi.org/10.1039/c9ta09377j.

[4] K.K. Fu, J. Cheng, T. Li, L. Hu, Flexible Batteries: From Mechanics to Devices, ACS Energy Lett. 1 (2016) 1065–1079.

[5] A.M. Gaikwad, A.C. Arias, Understanding the Effects of Electrode Formulation on the Mechanical Strength of Composite Electrodes for Flexible Batteries, ACS Appl. Mater. Interfaces. 9 (2017) 6390–6400, https://doi.org/10.1021/acsami.6b14719.

[6] G. Zhou, F. Li, H.-M. Cheng, Progress in flexible lithium batteries and future prospects, Energy Environ. Sci. 7 (2014) 1307–1338, https://doi.org/10.1039/ c3ee43182g.

[7] L. Hu, H. Wu, F. La Mantia, Y. Yang, Y. Cui, F. Secondary, L.P. Batteries, Thin, Flexible Secondary Li-Ion Paper Batteries, ACS Nano. 4 (2010) 5843–5848. https://doi.org/10.1021/nn1018158.

[8] W. Liu, M.-S. Song, B. Kong, Y. Cui, Flexible and Stretchable Energy Storage: Recent Advances and Future Perspectives, Adv. Mater. 29 (2017) 1603436, https://doi. org/10.1002/adma.201603436.

[9] C.F. Du, Q. Liang, Y. Luo, Y. Zheng, Q. Yan, Recent advances in printable secondary batteries, J. Mater. Chem. A. 5 (2017) 22442–22458, https://doi.org/10.1039/ c7ta07856k.

[10] K. Choi, D.B. Ahn, S.Y. Lee, Current Status and Challenges in Printed Batteries: Toward Form Factor-Free Monolithic Integrated Power Sources, ACS Energy Lett. 3 (2018) 220–236.

[11] N. Singh, C. Galande, A. Miranda, A. Mathkar, W. Gao, A.L.M. Reddy, A. Vlad, P.M. Ajayan, Paintable battery, Sci. Rep. 2 (2012) 6–10, https://doi.org/10.1038/ srep00481.

[12] X. Han, Z. Zhao, Y. Xu, D. Liu, H. Zhang, C. Zhao, Synthesis and characterization of F-doped nanocrystalline Li 4 Ti 5 O 12 /C compounds for lithium-ion batteries, RSC Adv. 4 (2014) 41968–41975, https://doi.org/10.1039/C4RA04953E.

[13] J.P. Bourgeois, A. Vlad, S. Melinte, J.F. Gohy, Design of Flexible and Self-Standing Electrodes for Li-Ion Batteries, Chinese J. Chem. 35 (2017) 41–47, https://doi.org/ 10.1002/cjoc.201600521.

[14] L. Huang, Q. Guan, J. Cheng, C. Li, W. Ni, Z. Wang, Y. Zhang, B. Wang, Freestanding N-doped carbon nanofibers/carbon nanotubes hybrid film for flexible, robust half and full lithium-ion batteries, Chem. Eng. J. 334 (2018) 682–690, https://doi.org/10.1016/j.cej.2017.10.030.

[15] J. Ren, R.P. Ren, Y.K. Lv, A flexible 3D graphene@CNT@MoS 2 hybrid foam anode for high-performance lithium-ion battery, Chem. Eng. J. 353 (2018) 419–424, https://doi.org/10.1016/j.cej.2018.07.139.

[16] K. Zhu, H. Gao, G. Hu, A flexible mesoporous Li4Ti5O12-rGO nanocomposite film as free-standing anode for high rate lithium ion batteries, J. Power Sources. 375 (2018) 59–67, https://doi.org/10.1016/j.jpowsour.2017.11.053.

[17] Y. Wang, H. Liao, J. Wang, X. Qian, Y. Zhu, S. Cheng, Effects of current collectors on electrochemical performance of FeS2 for Li-ion battery, Int. J. Electrochem. Sci. 8 (2013) 4002–4009, https://doi.org/10.1016/j.jpowsour.2011.09.014.

[18] F. Bahmani, S.H. Kazemi, Y. Wu, L. Liu, Y. Xu, Y. Lei, CuMnO2-reduced graphene oxide nanocomposite as a free-standing electrode for high-performance supercapacitors, Chem. Eng. J. 375 (2019) 121966,, https://doi.org/10.1016/j.cej.2019. 121966.

[19] Y. Qian, X. Cai, C. Zhang, H. Jiang, L. Zhou, B. Li, L. Lai, A free-standing Li4Ti5O12/ graphene foam composite as anode material for Li-ion hybrid supercapacitor, Electrochim. Acta. 258 (2017) 1311–1319, https://doi.org/10.1016/j.electacta. 2017.11.188.

[20] D.V. Carvalho, N. Loeffler, G.T. Kim, M. Marinaro, M. Wohlfahrt-Mehrens, S. Passerini, Study of water-based lithium titanate electrode processing: The role of pH and binder molecular structure, Polymers (Basel). 8 (2016) 1–2, https://doi. org/10.3390/polym8080276.

[21] D.V. Carvalho, N. Loeffler, M. Hekmatfar, A. Moretti, G.T. Kim, S. Passerini, Evaluation of guar gum-based biopolymers as binders for lithium-ion batteries electrodes, Electrochim. Acta. 265 (2018) 89–97, https://doi.org/10.1016/j. electacta.2018.01.083.

[22] F. De Giorgio, A. La Monaca, A. Dinter, M. Frankenberger, K.H. Pettinger, C. Arbizzani, Water-processable Li4Ti5O12 electrodes featuring eco-friendly sodium alginate binder, Electrochim. Acta. 289 (2018) 112–119, https://doi.org/10.1016/j.electacta.2018.09.017.

[23] V.V.N. Phanikumar, V.R. Rikka, B. Das, R. Gopalan, B.V.A. Rao, R. Prakash, Investigation on polyvinyl alcohol and sodium alginate as aqueous binders for lithium-titanium oxide anode in lithium-ion batteries, Ionics (Kiel). 25 (2019) 2549–2561, https://doi.org/10.1007/s11581-018-2751-8.

[24] T.C. Nirmale, B.B. Kale, A.J. Varma, A review on cellulose and lignin based binders and electrodes: Small steps towards a sustainable lithium ion battery, Int. J. Biol. Macromol. 103 (2017) 1032–1043, https://doi.org/10.1016/j.ijbiomac.2017.05. 155.

[25] H. Chen, M. Ling, L. Hencz, H.Y. Ling, G. Li, Z. Lin, G. Liu, S. Zhang, Exploring Chemical, Mechanical, and Electrical Functionalities of Binders for Advanced Energy-Storage Devices, Chem. Rev. 118 (2018) 8936–8982.

[26] J.T. Li, Z.Y. Wu, Y.Q. Lu, Y. Zhou, Q. Sen Huang, L. Huang, S.G. Sun, Water Soluble Binder, an Electrochemical Performance Booster for Electrode Materials with High Energy Density, Adv. Energy Mater. 7 (2017) 1–30, https://doi.org/10.1002/aenm. 201701185.

[27] A. García, M. Culebras, M.N. Collins, J.J. Leahy, Stability and rheological study of sodium carboxymethyl cellulose and alginate suspensions as binders for lithium ion batteries, J. Appl. Polym. Sci. 135 (2018) 11–13, https://doi.org/10.1002/app.46217.

[28] H.K. Park, B.S. Kong, E.S. Oh, Effect of high adhesive polyvinyl alcohol binder on the anodes of lithium ion batteries, Electrochem. Commun. 13 (2011) 1051–1053, https://doi.org/10.1016/j.elecom.2011.06.034.

[29] B. Tran, I.O. Oladeji, Z. Wang, J. Calderon, G. Chai, D. Atherton, L. Zhai, Adhesive PEG-based binder for aqueous fabrication of thick Li4Ti5O12electrode, Electrochim. Acta. 88 (2013) 536–542, https://doi.org/10.1016/j.electacta.2012.10.139.

[30] M. Gao, C.C. Shih, S.Y. Pan, C.C. Chueh, W.C. Chen, Advances and challenges of green materials for electronics and energy storage applications: from design to endof-life recovery, J. Mater. Chem. A. 6 (2018) 20546–20563, https://doi.org/10.1039/C8TA07246A.

[31] D. Bresser, D. Buchholz, A. Moretti, S. Passerini, A. Varzi, D. Buchholz, Alternative binders for sustainable electrochemical energy storage – the transition bio-derived polymers, Energy Environ. Sci. 11 (2018) 3096–3127, https://doi.org/10.1039/ c8ee00640g.

[32] C. Piffet, F. Boschini, R. Cloots, Flexible thin-films for battery electrodes, WO2018141659A1, 2018.

[33] T.-F. Yi, S.-Y. Yang, Y. Xie, Recent advances of $Li_4Ti_5O_{12}$ as a promising next generation anode material for high power lithium-ion batteries, J. Mater. Chem. A. 3 (2015) 5750–5777, https://doi.org/10.1039/C4TA06882C.

[34] X. Sun, P.V. Radovanovic, B. Cui, Advances in spinel Li4Ti5O12 anode materials for lithium-ion batteries, New J. Chem. 39 (2015) 38–63, https://doi.org/10.1039/ c4nj01390e.

[35] G. Xu, P. Han, S. Dong, H. Liu, G. Cui, L. Chen, Li4Ti5O12-based energy conversion and storage systems: Status and prospects, Coord. Chem. Rev. 343 (2017) 139–184, https://doi.org/10.1016/j.ccr.2017.05.006.

[36] Y. Liu, X. Yan, B. Xu, J. Lan, Y. Yu, X. Yang, Y. Lin, C. Nan, Li 4 Ti 5 O 12 nanosheets assembled in tubular architecture for lithium storage, Chem. Eng. J. 361 (2019) 1371–1380, https://doi.org/10.1016/j.cej.2018.10.185.

[37] F. Khan, M. Oh, J.H. Kim, N-functionalized graphene quantum dots: Charge transporting layer for high-rate and durable Li4Ti5O12-based Li-ion battery, Chem. Eng. J. 369 (2019) 1024–1033, https://doi.org/10.1016/j.cej.2019.03.161.

[38] C. Fongy, P. Moreau, S. Chazelle, M. Bouvier, S. Jouanneau, D. Guyomard, B. Lestriez, Toward the Aqueous Processing of Li4Ti5O12: A Comparative Study with LiFePO4, J. Electrochem. Soc. 159 (2012) A1083–A1090, https://doi.org/10. 1149/2.075207jes.

[39] H. Jung, J. Kim, B. Scrosati, Y. Sun, Micron-sized, carbon-coated Li 4 Ti 5 O 12 as high power anode material for advanced lithium batteries, J. Power Sources. 196 (2011) 7763–7766, https://doi.org/10.1016/j.jpowsour.2011.04.019.

[40] K. Nakahara, R. Nakajima, T. Matsushima, H. Majima, Preparation of particulate Li 4 Ti 5 O 12 having excellent characteristics as an electrode active material for power storage cells, 117 (2003) 131–136. https://doi.org/10.1016/S03787753(03)00169-1.

[41] C. Jamin, T. Jungers, C. Piffet, A. Mahmoud, R. Cloots, B. Vertruyen, F. Boschini, Li4Ti5O12 powders by spray-drying: Influence of the solution concentration and particle size on the electrochemical properties, J. Phys. Conf. Ser. 1081 (2018) 012001,, https://doi.org/10.1088/1742-6596/1081/1/012001.

[42] B. Vertruyen, N. Eshraghi, C. Piffet, J. Bodart, A. Mahmoud, F. Boschini, Spraydrying of electrode materials for lithium- and sodium-ion batteries, Materials (Basel). 11 (2018) 1076, https://doi.org/10.3390/ma11071076.

[43] J. Li, B.L. Armstrong, C. Daniel, J. Kiggans, D.L. Wood, Optimization of multicomponent aqueous suspensions of lithium iron phosphate (LiFePO4) nanoparticles and carbon black for lithium-ion battery cathodes, J. Colloid Interface Sci. 405 (2013) 118–124, https://doi.org/10.1016/j.jcis.2013.05.030.

[44] R.W. Cheary, A. Coelho, Fundamental parameters approach to x-ray line-profile fitting, J. Appl. Crystallogr. 25 (1992) 109–121, https://doi.org/10.1107/ S0021889891010804.

[45] I.C. Madsen, N.V.Y. Scarlett, A. Kern, Description and survey of methodologies for the determination of amorphous content via X-ray powder diffraction, Zeitschrift Fur Krist. 226 (2011) 944–955, https://doi.org/10.1524/zkri.2011.1437.

[46] D.R. Simon, E.M. Kelder, M. Wagemaker, F.M. Mulder, J. Schoonman, Characterization of proton exchanged Li4Ti5O12 spinel material, Solid State Ionics. 177 (2006) 2759–2768, https://doi.org/10.1016/j.ssi.2006.03.057.

[47] Y. Gao, Z. Wang, L. Chen, Stability of spinel Li4Ti5O12in air, J. Power Sources. 245 (2014) 684–690, https://doi.org/10.1016/j.jpowsour.2013.07.031.

[48] C. Te Hsieh, I.L. Chen, Y.R. Jiang, J.Y. Lin, Synthesis of spinel lithium titanate anodes incorporated with rutile titania nanocrystallites by spray drying followed by calcination, Solid State Ionics. 201 (2011) 60–67, https://doi.org/10.1016/j.ssi. 2011.08.002.

[49] H. Ge, L. Cui, Z. Sun, D. Wang, S. Nie, S. Zhu, B. Matthews, G. Wu, X.M. Song, T.Y. Ma, Unique Li4Ti5O12/TiO2 multilayer arrays with advanced surface lithium storage capability, J. Mater. Chem. A. 6 (2018) 22053–22061, https://doi.org/10.1039/c8ta03075h.

[50] Sigma aldrich IR spectra database, (2020). https://www.sigmaaldrich.com/ technical-documents/articles/biology/ir-spectrum-table.html.

[51] B.W. Chieng, N.A. Ibrahim, W.M.Z.W. Yunus, M.Z. Hussein, Poly(lactic acid)/poly (ethylene glycol) polymer nanocomposites: Effects of graphene nanoplatelets, Polymers (Basel). 6 (2014) 93–104, https://doi.org/10.3390/polym6010093.

[52] M.W. Davies, R. Shields, An infrared spectrophotometric method of estimating polyethylene glycol 4000, Gut. 9 (1968) 617–619, https://doi.org/10.1136/gut.9.5.617.

[53] K. Shameli, M. Bin Ahmad, S.D. Jazayeri, S. Sedaghat, P. Shabanzadeh, H. Jahangirian, M. Mahdavi, Y. Abdollahi, Synthesis and characterization of polyethylene glycol mediated silver nanoparticles by the green method, Int. J. Mol. Sci. 13 (2012) 6639–6650. https://doi.org/10.3390/ijms13066639.

[54] M. Rozenberg, A. Loewenschuss, Y. Marcus, IR spectra and hydration of short-chain polyethyleneglycols, Spectrochim. Acta - Part A Mol. Biomol. Spectrosc. 54 (1998) 1819–1826. https://doi.org/10.1016/S1386-1425(98)00062-6.

[55] H. Parant, G. Muller, T. Le Mercier, J.M. Tarascon, P. Poulin, A. Colin, Flowing suspensions of carbon black with high electronic conductivity for flow applications: Comparison between carbons black and exhibition of specific aggregation of carbon particles, Carbon N. Y. 119 (2017) 10–20, https://doi.org/10.1016/j.carbon.2017.04.014.

[56] Y. Li, W. Wu, F. Lin, A. Xiang, The Interaction Between Poly(vinyl alcohol) and Low-Molar-Mass Poly(ethylene oxide), J. Appl. Polym. Sci. 126 (2012) 162–168, https://doi.org/10.1002/app.3508.

[57] G. Hirankumar, N. Mehta, Effect of incorporation of different plasticizers on structural and ion transport properties of PVA-LiClO 4 based electrolytes, Heliyon. 4 (2018) e00992,, https://doi.org/10.1016/j.heliyon.2018.e00992.

[58] A. Shujahadeen B., W. Thompson J., K. M.F.Z., A. Hameed M., A conceptual review on polymer electrolytes and ion transport models, J. Sci. Adv. Mater. Devices. 3 (2018) 1–17. https://doi.org/10.1016/j.jsamd.2018.01.002.

[59] S.W. Han, J.H. Ryu, J. Jeong, D.H. Yoon, Solid-state synthesis of Li4Ti5O12for high power lithium ion battery applications, J. Alloys Compd. 570 (2013) 144–149, https://doi.org/10.1016/j.jallcom.2013.03.203.

[60] Z. He, Z. Wang, F. Wu, H. Guo, X. Li, X. Xiong, Spherical Li 4 Ti 5 O 12 synthesized by spray drying from a different kind of solution, J. Alloys Compd. 540 (2012) 39–45, https://doi.org/10.1016/j.jallcom.2012.06.044.

[61] F. De Giorgio, A. La Monaca, A. Dinter, M. Frankenberger, K.H. Pettinger, C. Arbizzani, Water-processable Li4Ti5O12electrodes featuring eco-friendly sodium alginate binder, Electrochim. Acta. 289 (2018) 112–119, https://doi.org/10.1016/ j.electacta.2018.09.017.

[62] L. Ma-Hock, V. Strauss, S. Treumann, K. Küttler, W. Wohlleben, T. Hofmann, S. Gröters, K. Wiench, B. van Ravenzwaay, R. Landsiedel, Comparative inhalation toxicity of multi-wall carbon nanotubes, graphene, graphite nanoplatelets and low surface carbon black, Part. Fibre Toxicol. 10 (2013), https://doi.org/10.1186/ 1743-8977-10-23.

[63] X. Shaomei Cao, Y. Feng, X. Song, H. Xue, M. Liu, J. Miao, L. Shi Fang, Integrated Fast Assembly of Free-Standing Lithium Titanate/Carbon Nanotube/Cellulose Nanofiber Hybrid Network Film as Flexible Paper-Electrode for Lithium-Ion Batteries, ACS Appl. Mater. Interfaces. 7 (2015) 10695–10701.

[64] S. Ni, J. Liu, D. Chao, L. Mai, Vanadate-Based Materials for Li-Ion Batteries: The Search for Anodes for Practical Applications, Adv. Energy Mater. 9 (2019) 1–33, https://doi.org/10.1002/aenm.201803324.

[65] S. Komaba, T. Ozeki, K. Okushi, Functional interface of polymer modified graphite anode, J. Power Sources. 189 (2009) 197–203, https://doi.org/10.1016/j.jpowsour.2008.09.092.

[66] Y. Jiang, X. Yan, Z. Ma, P. Mei, W. Xiao, Q. You, Y. Zhang, Development of the PEO Based Solid Polymer Electrolytes for All-Solid State Lithium Ion Batteries, Polymers (Basel) (2018) 1–13, https://doi.org/10.3390/polym10111237.